Growth Kinetics of the {10.4} Faces of Nitratine (NaNO₃)

Raúl Benages-Vilau, Marco Rubbo, Teresa Calvet, Miquel Àngel Cuevas-Diarte, and Dino Aquilano

Growth kinetics of the {10.4} faces of Nitratine (NaNO₃)

Raúl Benages-Vilau [1], Marco Rubbo[2], Teresa Calvet[1], Miquel Àngel Cuevas-Diarte[1], Dino Aquilano[2]*

[1] Dpt. Cristal·lografia, Mineralogia i Dipòsits Minerals, Facultat de Geologia, Universitat de Barcelona, c/Martí i Franquès, s/n 08028 Barcelona, Spain

[2] Dipartimento di Scienze della Terra, Università degli Studi di Torino, via V. Caluso 35, I-10125 Torino, Italy

Abstract.

In this paper we focus on the measurement of the normal growth rates (R_{104}) of {10.4} faces of nitratine (NaNO₃) single crystals under isothermal conditions in the temperature interval 288 – 297. 5K in order to unravel the rate determining steps during crystal growth, depending on the hydrodynamic conditions. Owing to the elevated solubility of nitratine in water, the supersaturated system is very sensitive to temperature variation. In this sense we have constructed a device to control the temperature (its accuracy is below 0.1 K) and the concentration throughout the experiments. We managed to measure the crystal growth of three symmetry equivalent {10.4} faces of NaNO₃ under different hydrodynamic conditions. We found that growth of these faces depend on different rate determining steps (being either surface or volume diffusion limited) according to their position with respect to the solution flow. Finally, some thermodynamic crystallization parameters have been calculated to assess the rate determining steps.

1. Introduction

NaNO₃, mineral nitratine, (space group $R\bar{3}c$: $a_0 = 5.07$; $c_0 = 16.83$ Å) shows a crystal structure consisting in alternating layers of Na^+ and NO_3^- ions, nitrate layers being rotated each other by 60° around the triad axis.[1] Each Na^+ is octahedrally coordinated with oxygen atoms. Nitratine is iso-structural with calcite but its athermal equilibrium shape (ES), calculated using a semi-empirical potential[2], is very different from that of calcite as only the {10.4} cleavage rhombohedron is present because its surface energy is very low with respect to that of the other crystal forms. NaNO₃ is easy crystallized from an aqueous solution and the {10.4} rhombohedron always appears.

NaNO₃ single crystal growth has not been widely studied over the past years. The earliest research was by Sipyagin and Chernov[3] who measured the growth rate (R), in the interval 0-50°C at a constant undercooling of 0.3 °C and found an anomalous not monotonic increase in the linear crystal growth rate with temperature. Some years later, Kirkova and Nikolaeva[4] measured the growth rate as a function of the flow rate, at different supersaturation (σ) values. Results were essentially the same as reported by Sipyagin and Chernov. In both cases the indexes of the growing faces were ambiguous; further, the non-isothermal (R vs σ) measurements did not allow to evaluate the activation energy which is an important parameter controlling the crystal growth dynamics.

Ongoing, Treivus [5] put forward that the $NaNO_3$ growth from solution proceeds according to the dislocation mechanism in a convection free regime. Jones et al.[6-8] working at constant temperature but without controlling the supersaturation, developed a model which predicts the dependence between growth rate, dislocation density and strain. Moreover, studying the strain in $NaNO_3$ secondary nuclei as a function of supersaturation, proposed for the first time a Burton, Cabrera and Frank (BCF) isothermal model; unfortunately they did not work under isothermal conditions and hence the model they proposed results to be unreliable. Ristic et al.[9-10], using Michelson interferometry on strained crystals, were the first who measured a tangential growth rate of steps on the (10.4) faces of about 12 $\mu m\ s^{-1}$, at $\sigma = 0.2\%$. Finally, Graber et al. [11] studied the mass transfer and growth from aqueous solution in industrial crystallization, while Oosterhof et al. experimented with isopropoxyethanol-water mixtures.[12] Komnik and Startsev[13] (see also references therein) were the first to grow $NaNO_3$ single crystal from melt. More recently, Gopalakrishnan et al.[14] were able to grow 40×10 mm cylindrical $NaNO_3$ single crystals from melt (travelling zone method) with a dislocation density of about 10^3-10^4 cm^{-2}. Sawada and Shichiri[15] found that $NaNO_3$ crystals growing from the melt developed a non-faceted morphology at low undercooling and dendritic behavior at higher undercooling.

This short summary clearly shows that experimental data about crystal growth kinetics of $NaNO_3$, both from solution or melt, are rather scattered and not a single systematic approach has been attempted to date about the kinetics determining steps. Actually, at the best of our knowledge, no rigorous correlation has been obtained yet between the main surface property of a face (such as the specific edge energies), its normal growth rate, the supersaturations in the solution bulk and the crystallization temperature. Besides, any attempt has been made to investigate, at least qualitatively, the influence of the fluid dynamic regime on the growth rate.

Starting from a preliminary study on $NaNO_3$ crystal growth from aqueous solution [2], we aim at determining in this study experimental growth isotherms ($R_{(10.4)}$ vs σ), at three values of temperature, of the most important $NaNO_3$ form. At this end we will measure, simultaneously, the advancement rate of three equivalent (10.4) faces of the same single crystal. The measurements will be repeated using different crystal seeds in order to minimize the dispersion in the growth rate due to both the character and density of dislocations; it is worth mentioning that each experimental point onto a growth isotherm represents the average of ten measurements made under the same kinetic and hydrodynamic conditions. Then we will try to find the best fit between the experimental curves we obtained and the ones calculated by applying the classical theoretical models elaborated for the growth from solution which allow to discriminate the rate determining steps controlling crystal growth. Peculiar attention will be paid to the influence of the hydrodynamics on the growth rate of the simultaneously growing faces which are crystallographically equivalent, but are differently oriented with respect to the incoming solution flow.

2. Growth apparatus and materials

Our goal is to measure the normal crystal growth rate ($R_{10.4}$) under isothermal conditions in the temperature interval 288 - 297.5 K. For each isotherm, the temperature of crystallization (T_{growth}) is maintained constant while supersaturation is varied by changing the saturation temperature (T_{eq}) of the growth solution. This method[16] allows an unambiguous and very precise determination of the thermodynamic supersaturation $\Delta\mu = kT_{growth} \times \ln(1+\sigma)$, where it is $(1 + \sigma) = \dfrac{a(T_{growth})}{a(T_{growth})_{eq}}$ and $a(T_{growth})$ is the activity of a solution saturated at T_{eq}. The temperature interval $\Delta T = (T_{eq} - T_{growth})$, corresponding to the supersaturation range we choose, is $0.1 < \Delta T < 0.8$ K. It is worth to remember here that 3D-nucleation occurs when setting $\Delta T \geq 0.4$K, so the zone where crystals only grow is very narrow, as was already determined by Benages et al.[2] This requires an experimental setup designed to avoid depletion of the supersaturated solution by 3D-nucleation.

2.1. The experimental setup.

In order to measure the growth rate of the faces we have constructed a device to observe the face advancement under a microscope. Its diagram is shown in figure 1 together with a picture.
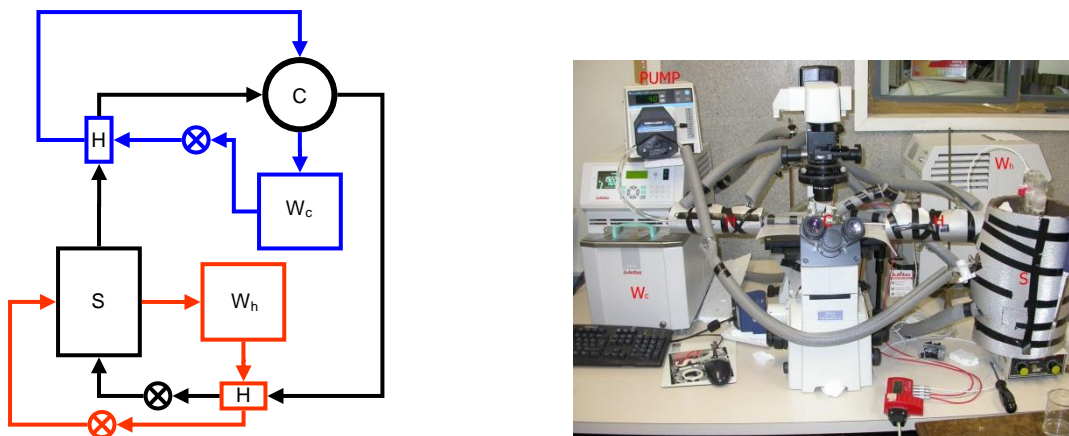

Figure 1. Flow diagram (left) and photo (right) of the home made growth cell device. Observation cell (C), peristaltic pump ($\otimes$, pump), thermostat baths (W_h, W_c), counter current concentric tube heat exchangers (H) and a reservoir (S).

The unit consists in five main bodies: an observation cell (C), a peristaltic pump ($\otimes$ or PUMP in the photo), two thermostatic baths (W_h, W_c) with two counter-current concentric tube heat exchangers (H) and a reservoir (S). As shown in Figure 1, the whole system is thermally insulated to avoid temperature fluctuations. The device has been built in AISI 304 stainless steel due to corrosive properties of $NaNO_3$ solutions. The reservoir was built in glass and the connections and valves were of polypropylene, finally tubing was of PVC and Tygon® for the pump section. The solution flows through the cell internal section of $0.6 \times 1 cm^2$. In order to maintain the temperature constant, the cell is encapsulated in a double-walled stainless steel circular block where water circulates at the desired temperature. The seed glued on the sample holder can be observed between two glass windows

mounted with "viton" gaskets. In the back part there are two temperature probes. The sample holder is a cylinder ending in a conical tip on which the crystal seed is glued and fixed; the holder is shaped to permit to rotate the crystal 360° around the direction perpendicular with respect to the flow inside the cell, in order to obtain the selected orientation. The solution reservoir buffers the concentration of the solution during measurements. The reservoir is a double-walled 1.3 liter vessel provided with temperature setting and monitoring. To change the supersaturation, water is added directly into the reservoir to achieve the desired saturation temperature T_{eq} and $\Delta T = (T_{eq} - T_{growth})$. This is repeated until T_{eq} becomes equal to T_{growth}. Two thermostatic baths control the temperature in the system. The first one is connected to one heat exchanger and to the growth cell in order to maintain constant the temperature inside it during the experiments. The other thermostat is used to prevent crystallization in the reservoir and to heat the solution (with the aid of a heat exchanger) just after the solution passed through the cell. The reservoir temperature is only adjusted when T_{growth} is varied to obtain a new set of isothermal growth rates. The temperature on the crystal maintained constant (its standard deviation being less than 0.05K), as measured by to two probes that are inserted, into the cell, just before and after the growing seed , at a distance of about 5 mm. A third probe monitors the temperature into the cooling bath and a fourth one is immersed into the solution reservoir; in the whole system the temperature is recorded every 5 seconds .

2.2 Source of material

$NaNO_3$ (analytical grade) was purchased at Quality Chemicals. According to the manufacturer, the major impurities are phosphor and sulfur atoms. Its purity was checked by ionic coupled plasma (ICP) with a mass detector; we have additionally found 21.7 ppm of titanium and 0.22 ppm of manganese. Powder X-ray diffraction confirmed that the product is a single II-$NaNO_3$ phase.2.3

2.3 Preparation of seed crystals

Seed crystals were grown by water evaporation of a saturated solution at 291 K; the crystallization process takes at least 2 days. Crystals of less than $2\times2\times1mm^3$ were picked up with tweezers from the solution, dried onto a filter paper and stored at room temperature; then, the best ones were glued on the sample holder tip with a 2 components epoxy resin. We used a magnifying glass to assure that the crystal is properly glued on the sample holder.

2.4.1 Batch preparation.

For solution preparation we relied on the solubility curve determined by Xu and Pruess[17]:

$$X = 0.0022 \times T - 0.1757 \qquad (1)$$

X being the mass fraction and T the absolute temperature[1]. We weighted the required amounts of water and sodium nitrate to have 1600 g of solution. The solution was vacuum filtered into the reservoir where the temperature was set above the predicted equilibrium temperature (T_{eq}) by the aid of the second thermostat to avoid any crystallization during the filtration. We prepared two

---

[1] We verified the consistency of these data with those by Archer used in the following to calculate the supersaturation of the solutions.

batches: the first one was used to measure the crystal growth at T_{growth} = 288 K and the second at T_{growth} = 297.5 K and, after dilution, at T_{growth} = 292.5 K.

2.4.2 Seed crystal mounting and hydrodynamics

First, we have to explain why we chose to avoid to grow the seed crystals in stagnant or quasi-stagnant solution. The main reason is that, under these conditions, different concentration gradients do arise along the growing surfaces, giving rise to morphological instabilities on the surface profiles, so vanishing the reliability of any kinetic measurement. Secondly, when only natural convection sets up, spontaneous plumes generate in the solution bulk and, consequently, strong discontinuities in the supersaturation values are produced onto the growing surfaces. Then, we decided to work under gentle hydrodynamic solution flow (2.35 cm×s^{-1}) . The rhombohedral shape of the seed does not allow getting, simultaneously, a face completely parallel to the solution flow and the other one perpendicular to it. Therefore, we chose a compromise in which the faces "normal" and "parallel" to the flow form an angle of $\approx$ 69° and $\approx$12° with respect to the flow direction, respectively; this in order to minimize the effect of turbulent regime on the "parallel" face due to the presence of the first exposed crystal edge, formed by parallel and normal faces, encountered by the incoming solution flow. One could object that the two opposite "normal" faces (labeled with + and − in Figure 2) are not equally fed by the solution. As a matter of fact, the face in front of the flow (+) should have a thinner boundary layer in respect to the opposite (−) one: for this reason we assumed that the growth rate (R^N_{104}) of the normal faces is the ratio ($\Delta d^N/\Delta t$) between the increment of the distance (Δd^N) of (+) and (−) faces and the elapsed time Δt . We are conscious that averaging the growth rates of the opposite faces represents an approximation of the "true" R^N_{104} value. Nevertheless, we know that this is the best way to monitor, simultaneously and on the same crystal, the growth of three symmetry equivalent faces at the same crystallization temperature. It can be said, *a posteriori*, that we made the right mix (hydrodynamic regime, crystal orientation) since we controlled *ex situ* the as grown surfaces and found that all of them where microscopically planar and brilliant, as it is typical of the flat (F) faces that did not suffer morphological instabilities.
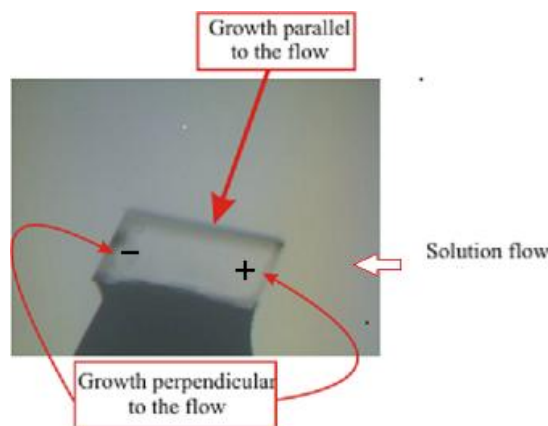
Figure 2. NaNO$_3$ crystal in the growth cell. Three symmetry equivalent faces of the same cleavage rhombohedron are simultaneously exposed to the solution flow: one parallel (P, R_{104}^p) and two perpendicular (N, R_{104}^N) faces with respect to the flow.

3. Calculation of the supersaturation of the solution

The calculation is based on the work by D.G. Archer[18] who used his modified Pitzer model of ionic solutions to parameterize the equilibrium properties of the system NaNO$_3$ −H$_2$O. We calculated the mean activity coefficient as a function of the solution ionic strength and its molality at the temperature of interest. In this sense, we prepared solutions and determined experimentally the saturation temperature according to Boistelle's procedure[19]. Then we relied on a spline interpolation of the equilibrium data between 273.15 and 373.15 K given in Archer's paper to obtain the thermodynamic relevant quantities.

The supersaturation at T$_{growth}$ is defined as $\sigma = \dfrac{a_{Na^+} \cdot a_{NO_3^-}}{(a_{Na^+} \cdot a_{NO_3^-})_{Tg}} - 1$, where the numerator contains the actual value of the NaNO$_3$ concentration, in term of molality (m$_{eq}$), and the denominator represents the NaNO$_3$ concentration at the crystallization temperature (m$_{growth}$). The experimental values of the growth rate for perpendicular (R_{104}^N) and parallel (R_{104}^p) faces at the three growth temperatures together with the supersaturation values are given in Table 1. At every supersaturation, the measurements of both crystal size and growth rates were repeated ten times.

Table 1. Experimental growth rate at different supersaturations (σ) for perpendicular (R_{104}^N) and parallel (R_{104}^p) faces at the three temperatures of growth.

ΔT (K)	σ ×10^{-3}	R_{104}^N ×10^{-7}cm/s	R_{104}^p ×10^{-7} cm/s
		288.0 K	
0.1	1.401	1.07	1.17
0.2	2.804	3.28	2.57
0.4	5.616	5.85	6.48
0.5	7.023	6.80	8.12
		292.5 K	
0.2	2.767	4.03	4.50
0.3	4.153	5.07	3.48
0.4	5.540	9.58	8.47

0.5	6.929	11.5	9.65
297.5 K			
0.2	2.712	7.62	6.58
0.3	4.070	7.02	9.22.
0.4	5.430	15.8	22.9
0.5	6.791	21.5	19.9
0.7	9.519	23.5	16.5
0.8	10.88	37.5	26.7

4. Measured growth isotherms

To identify the growth mechanism describe the dependence of the growth rate on supersaturation of the $NaNO_3$ {10.4} faces (N, perpendicular to the solution flow and P, parallel), we refer to the work by Gilmer, Ghez and Cabrera (GGC hereinafter) [20] who considered the stationary growth of a crystal due to combined volume and surface diffusion processes. Accordingly, the more general form of a face growth rate depends on the slope of the growth hillocks, on transport properties in the bulk of the solution and crystal surface and on the kinetics of integration of the growth unit in the steps. Depending on the relative weight of volume and surface diffusion and rate of integration of growth units in the steps, the general (R vs σ) relation assumes specialized forms recovering the relations proposed by Burton, Cabrera, Frank (BCF hereinafter), [21] Bennema and Gilmer[22] and Chernov. [23]

The GGC master equation reduces to eq (2) in the case where the mean free path of growth units in solution, Λ, is much greater than that on the crystal face, λ. Then, $\frac{\lambda}{\Lambda} \to 0$ is expected as surface diffusion requires desorption of the growth units. This assumption will be here justified *a posteriori*, if we find a relationship R vs. σ acceptable under this assumption.

$$R_{hkl} = \frac{N_0\,\Omega D_v \sigma}{\Lambda + \delta + \frac{\Lambda \Lambda_s l}{\lambda^2} + \Lambda[\frac{l}{2\lambda} coth\frac{l}{2\lambda} - 1]} \qquad (2)$$

The meanings of the symbols in equation (2) are:
N_0 density of solute at equilibrium,
Ω volume of a formula unit in the crystal cell, $\Omega = 62.40530 \times 10^{-24}\ cm^3$.
D_v diffusion coefficient of growth units in solution,
σ supersaturation of the solution,
Λ mean free path of a growth unit in solution,

δ thickness of the boundary layer

Λ_s coefficient related to the transfer of growth units between steps and surface,

λ mean free path of a growth unit on crystal face,

l equidistance of steps

τ_s the life time of a growth unit on the crystal surface before desorption.

The terms in the denominator are impedances to the growth rate which are, in the order: the first, the impedance of the adsorption reaction; the second the impedance to enter in the unstirred layer; the third the impedance for entering the steps and the forth as the surface diffusion impedance.

5 Determination of the growth model and energy parameters.

As we have to do with three equivalents {10.4} faces growing under different hydrodynamic conditions, we ought analyzing them separately. We first sought with the two faces perpendicular to the incoming flow and, after that, with the parallel one. In this part we determine as well the most probable rate determining steps and some thermodynamic parameters that help us to validate the proposed theories. As the positive and negative crystal faces having orientation perpendicular to the solution flow, keep a flat and stable surface during growth, we treat them as experiencing the same thickness of the boundary layer. This assumption is consistent with the measurement of the mean growth rate of the positive and negative faces and can be justified considering that the rate of flow of the solution is slow and then the diffusion of the growth units in the solution potentially can limit the growth of the N faces, irrespectively of their orientation. This assumption can lead us to overestimate the weight of the volume diffusion on the positive N faces and of the surface diffusion on the negative N faces: as we will see, the consequence is that we calculate a kind of mean value of the quantity $\frac{\gamma a^2}{kT\lambda}$ discussed in the following. However, the rate limiting step should be correctly identified.

5.1 Faces perpendicular to the solution flow (N)

We start with the analysis of the growth curves (R_{104}^N vs σ) of the faces perpendicular to the solution flow. Indeed, the variation of the growth rates of the face parallel to the flow (R_{104}^P vs σ) shows a different behavior with temperature and supersaturation and will be analyzed in a second moment. In order to identify a growth rate limiting step we tested different hypotheses, as detailed in the following.

5.1.1 Chernov model

Because the measured growth rates suggest a linear increase of the growth rate with supersaturation, we tested at first if the growth is limited by volume diffusion. When the volume diffusion parameter is larger than the thickness of boundary layer ($\Lambda \gg \delta$), equation (2) transform to equation (3) which represents the Chernov model, i.e. the growth rate determined by volume diffusion

$$R = \frac{N_0 \, \Omega D_v \sigma}{\Lambda(\frac{\Lambda_s l}{\lambda^2} + \frac{l}{2\lambda} \coth \frac{l}{2\lambda})}; \qquad (3)$$

Two a-dimensional parameters were determined by non-linear least squares:

$p_2 = \sigma \frac{l}{2\lambda} = \frac{\gamma a}{kT\lambda}$ and $p_1 = \frac{2\Lambda_s}{\lambda}$, **where γ** is the mean specific edge energy (erg cm^{-1}) of a 2D-nucleus on a (10.4) face and a the area (cm^2) occupied by the growth unit on the step ledge. At

297.5 K, the diffusion coefficient $D \cong 1.03 \cdot 10^{-5}$, was calculated by the Nernst equation considering its variation with concentration: $D_v = D^0(1 + \frac{d\log(\gamma_{\pm})}{d\log(c)})$. The data to calculate D^0 are from Robinson and Stokes reporting the values of the limiting equivalent conductivities:[24]

$$D^0 = \frac{RT}{F^2}\frac{v_1 + v_2}{v_1|z_1|}\frac{\lambda_1^0\lambda_2^0}{\lambda_1^0 + \lambda_2^0}$$

Here, v_1 and v_2 correspond to the number of cations, algebraic valence z_1 and anions, algebraic valence z_2 , generated by the dissociation of a unit formula of electrolyte. λ_i^0 are the limiting equivalent conductivities, R and F are the gas and Faraday constant.

The values of Λ were fixed and spanned several order of magnitude. The least squares test was made on the isotherm at 297.5 K. Only for values $\Lambda \cong 9.10^{-3}cm$ the least squares converged: the values of the parameters are affected by high variance values, but this law cannot be rejected on the ground of a $\chi_{0.9}^2$ test with four degrees of freedom.[25] Anyway, we independently calculated the thickness of the boundary layer using the approximated expression given by GGC and derived by Carlson[26] :

$$\delta = \frac{3}{2}(\frac{kT\rho}{6\pi r\eta^2})^{\frac{1}{3}}(\frac{\eta d}{\rho v})^{\frac{1}{2}}$$

The values of density ρ and viscosity η, can be obtained using their parametric representations given in the paper by Xu and Pruess, and NIST.[17] The molecular size r is known, while the rate of flow of the solution v and the linear size of the crystal d, are experimental.

It turns out that δ is of the order of $10^{-3}cm$. As the Chernov model is obtained when $\Lambda \gg \delta$, which contradicts our finding, this model should be excluded. Furthermore we verified that the Chernov equation (3) cannot fit the other isotherms at 288.0K and 292.5K.

.

5.1.2 Growth limited by surface diffusion

When the surface diffusion is the rate limiting step, from equation (2) one obtains the BCF growth law limited by surface diffusion (BCF-S):

$$R_{104}^N = \frac{p_1}{p_2}\tanh(\frac{p_2}{\sigma}) \times \sigma^2 \qquad (4)$$

In equation (4), $p_1 = \frac{D_s\Omega n_{s0}}{\lambda_s^2} = \frac{n_0\Omega}{\tau}$ and $p_2 = \frac{\epsilon}{c}\frac{\gamma a^2}{kT\lambda}$ represent the parameters to be determined by least squares: D_s is the surface diffusion coefficient, λ_s the mean free path of the growth units on the crystal face, τ the residence time of a growth unit on the surface before desorption, γ the edge free energy, a^2 the area occupied by a growth unit in a mesh on a step, $\frac{c}{\epsilon}$ the ratio between the shape factor (c) of the growth spiral and the number of dislocation in a bundle (ϵ). n_{s0} is the concentration of adsorbed growth unit at equilibrium. Finally, $l = \frac{2\gamma a^2}{kT\sigma}$ is the mean distance between steps.

In the following we report the measured growth rates over which are superimposed the regression curves. The regression parameters and the statistical analyses are given in Table 2.

Table 2. BCF growth model parameters determined for $R^N_{(10.4)}$ growth rates at three temperatures.

	288.0K		292.5K		297.5K	
	Value	Error	Value	Error	Value	Error
p_1	$0.997 \cdot 10^{-4}$	$0.164 \cdot 10^{-4}$	$0.176 \cdot 10^{-3}$	$1.40 \cdot 10^{-4}$	$0.347 \cdot 10^{-3}$	$8.19 \cdot 10^{-5}$
p_2	$0.924 \cdot 10^{-3}$	$1.56 \cdot 10^{-3}$	$4.23 \cdot 10^{-3}$	$5.64 \cdot 10^{-3}$	$4.85 \cdot 10^{-3}$	$3.86 \cdot 10^{-7}$

In Figure 3 the BCF-S fitting to the experimental values for the three temperatures is shown (Blue: 297,5K; red: 292,5K; and green: 288,0K). It is worth to outline that:

-the so called parabolic branches of the curves are restricted to a very low supersaturation values, the lower the temperature the smaller the parabolic region;

-the transition from the "parabolic" to the "linear" branch is gradual as can be seen for the 297,5K isotherm (blue line);

We tested also a linear relationship (R vs σ): the χ^2 values calculated for each regression line are not significantly different from those calculated fitting the BCF eq. (2). In particular, at every temperature, the slope of the linear fits have values close to those of p_1 calculated from eq.(2). This is reasonable and so there are not statistical evidence to reject eq.(2). As the measurements fall in the region of transition from the "parabolic" to the "linear" branch of the curves R vs. σ (eq.2), the parameter p_1 is more constrained than p_2.
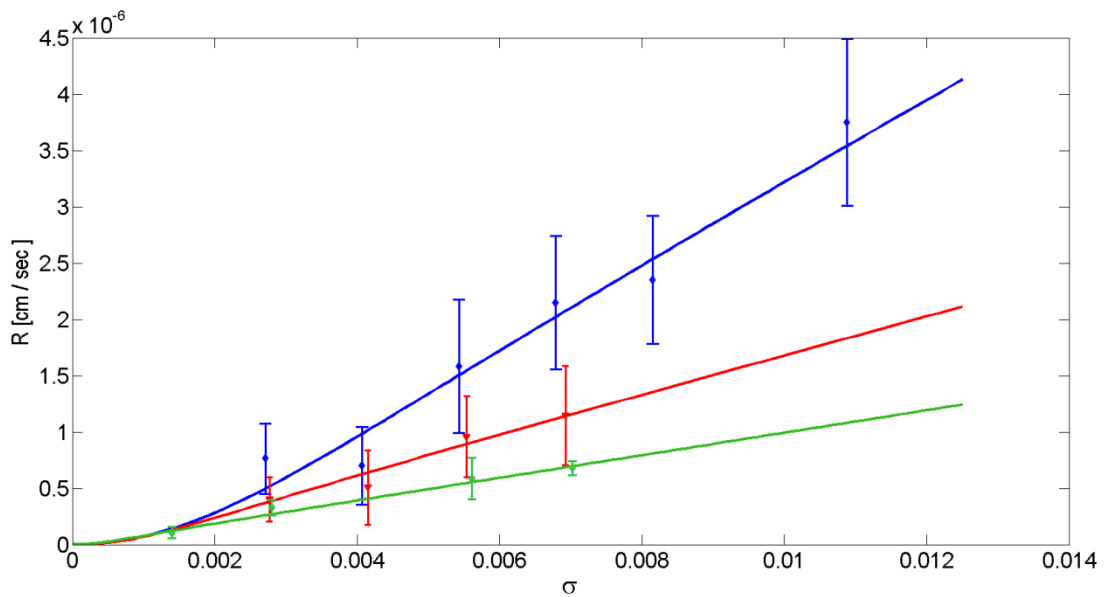

Figure 3. Experimental growth isotherms $R^N_{(10.4)}$ along with their theoretical BCF-S plots (Green: 288.0 K, Red: 292.5 K, Blue: 297.5 K)

We see in Figs. 3 and 4 that the standard errors affecting the measured rates increase with the temperature of the isotherms, as well as the dispersion of the measured points about the best fit curves. Carlson[26] pointed out that turbulent flow may lead to starvation of faces whose normal is perpendicular to the solution flow (in this paper faces P, see Fig.2) and convection plumes can lead to wedged crystals implying the formation of vicinal and even higher index faces.[27] As already detailed in section 2.4.2 , we imposed a slow solution flow to avoid uncontrolled convection; moreover, to keep similar hydrodynamic conditions the initial size and shape of the crystals was always the same.

Moreover, the models we use to unravel a growth model assume that the growth hillocks are made by a sequence of equal spaced steps as a consequence of neglecting the steps movements with respect to the rate of diffusion of the growth units towards the steps. As shown by the measurements on the face (10.4) of nitratine,[28] even single spiral sides do not have a constant slope. This can be understood considering that l, the equidistance between successive spiral steps, is proportional to the step curvature: $\rho_c \propto \frac{\gamma a}{\Delta \mu}$, close to the dislocation core, while near the spiral periphery the advancement rate of the steps is determined by crystal edges, steps from other sources, defects, etc. As a consequence, step bunching occurs, as also shown in some models[29] and theoretical works on the kinematic waves.[30] The bunching is enhanced with increasing temperature as the mean rate of advancement of the steps is higher. It follows that the measured growth rate of a crystal face is a mean over different domains of the same face where the steps density, and often their height, vary from site to site of the face. Finally, to measure a growth isotherm requires the use of several crystals what may cause growth rate dispersion, as far as each crystal has a different dislocations distribution and density. There is a temperature effect as well, because the generation of growth defects increases with the growth rate.

5.1.3 Growth limited by volume transport and surface diffusion

When imposing to equation (2) that the coefficient related to the transfer of growth units between steps and surface must be smaller than the mean free path onto the surface ($\Lambda_s \ll \lambda$) one obtains the equation:

$$R = \frac{N_0 \, \Omega D_v}{\delta + \Lambda \frac{l}{2\lambda} coth \frac{l}{2\lambda}} \times \sigma \qquad (5)$$

We refer to this coupling between volume and surface as the GGC-VS model. Using the estimated value of δ, we determined two parameters fitting this expression to the isotherms. The regression parameters and the statistical analyses are given in Table 3 and graphically shown in Figure 4. The parameter t_1 corresponds to Λ and t_2 to $\frac{\epsilon}{c} \frac{\gamma a^2}{kT\lambda}$.

Table 3. Parameters of volume and surface diffusion growth model, determined for $R^N_{(10.4)}$ growth rates at three temperatures. The parameter indicated with the symbol t_2 and p_2 in Table 2, represents the same physical quantity.

	288.0K		292.5K		297.5K	
	Value	Error	Value	Error	Value	Error
t_1	$0.196 \cdot 10^{-1}$	$2.08 \cdot 10^{-3}$	$0.112 \cdot 10^{-1}$	$8.95 \cdot 10^{-3}$	$0.524 \cdot 10^{-2}$	$2.08 \cdot 10^{-3}$
t_2	$0.995 \cdot 10^{-3}$	$1.70 \cdot 10^{-3}$	$5.18 \cdot 10^{-3}$	$7.55 \cdot 10^{-3}$	$6.77 \cdot 10^{-3}$	$5.60 \cdot 10^{-3}$

When $\frac{\delta}{\Lambda} \ll \frac{l}{2\lambda}$, at low supersaturation, the growth rate is approximately proportional to the square of the supersaturation. When, with increasing supersaturation, it becomes $\frac{l}{2\lambda} \ll \frac{\delta}{\Lambda}$ the relation between growth rate and supersaturation tends to be linear. At low supersaturation, the rate is limited by the surface processes while at higher supersaturation the rate is determined by volume diffusion. We observe that the equidistance between spiral arms, $l \propto \frac{\gamma a^2}{kT\sigma}$, is the parameters determining the change of curvature of both isotherms BCF, equation (4) and GGC-VS equation (5).
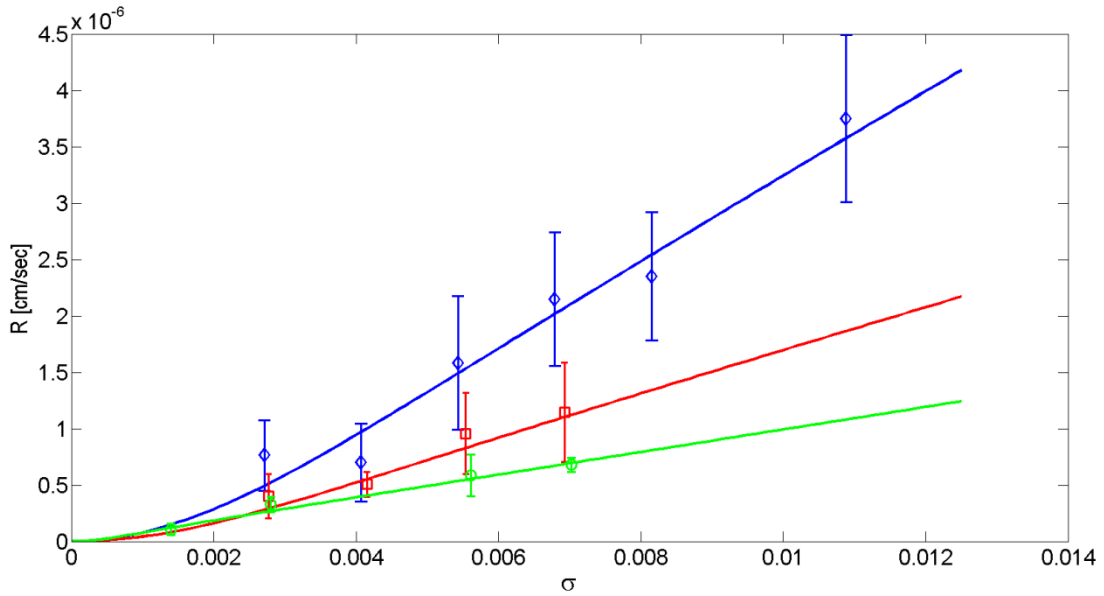

Figure 4. Experimental growth isotherms $R^N_{(10.4)}$ along with their theoretical GGC-VS plots (Green: 288.0 K,   Red: 292.5 K,   Blue: 297.5 K)

5.2 Face parallel to the solution flow (P).

We also sought to assess the step determining the growth rate of the face parallel to the incoming flow, as described in the following.

5.2.1 Growth limited by volume diffusion.

We did not try a fit with the BCF law used in case of the growth of the faces perpendicular to the solution flow. As the measured isotherms (Fig. 5) do not exhibit a curvature at low σ values, we tested a linear fit: $R = a \times \sigma$.
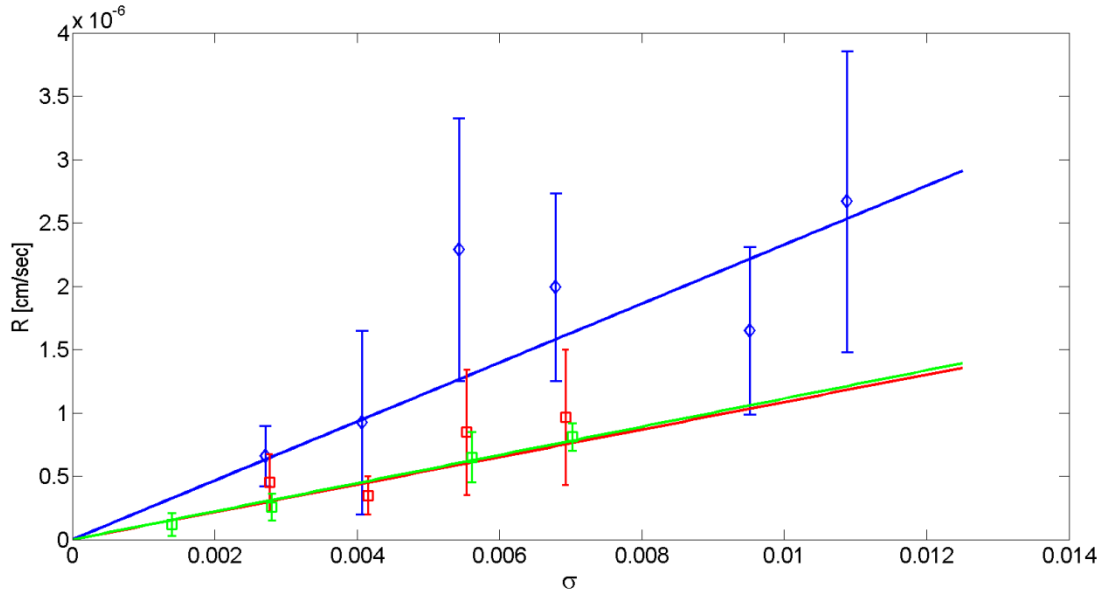

Figure 5. Experimental growth isotherms $R^P_{(10.4)}$ along with their linear representations (Green: 288.0 K, Red: 292.5 K, Blue: 297.5 K).

The linear law can be derived from equation (2) when l, the equidistance between steps, is very small with respect to the mean free path, Λ_s , on the surface ($l / \Lambda_s \to 0$): this means that surface diffusion is negligible with respect to the volume diffusion that becomes the rate determining process. Given this conditions, the denominator on equation (2) reduces to (δ+Λ) and hence the parameter a coincides with $\left(\frac{N_0\ \Omega D_v}{\delta+\Lambda}\right)$:

$$R = \left(\frac{N_0\ \Omega D_v}{\delta+\Lambda}\right) \times \sigma \qquad (6)$$

In eq. (6), N_0 is the equilibrium concentration of growth units in solution, Ω is the volume of a formula unit in the kinks, D_v is the diffusion coefficient in solution, δ the thickness of the solution boundary layer on the (10.4) face, while Λ , which is related to the free path of a growth unit in solution, is a retarding factor increasing with the activation energy for desolvation. The regression coefficient 'a' is given in the table 5.

From the regression coefficient, knowing $N_0\ \Omega D_v$ and Λ at the three values of temperature, we estimate the boundary layer thickness δ(P) over the P face. The δ(P) values are compared with the δ(N) ones derived from the formula by Carlson, for the three crystallization temperatures, respectively :

T crystallization (K)	288.0	292.5	297.5
δ(N) ×10^{-3} cm	3.151	3.201	3.254
δ(P) ×10^{-3} cm	0.761	12.82	7.675

Notwithstanding that on δ(P) propagates the error affecting the measures of the growth rates of the P face, the increase of the boundary layer thickness over the P face looks likely and this factor is limiting the growth rate.

In the next section, to further corroborate the proposed growth model, the dependence on temperature of the parameters estimated by statistical analysis can be checked and the value of same properties calculated.

Table 5. Calculated parameters for the linear law: isotherms (R^P_{104}).

	288.0 K		292.5 K		297.5 K	
	Value	Error	Value	Error	Value	Error
regression coefficient a (cm×s^{-1})	$1.11 \cdot 10^{-4}$	$1.30 \cdot 10^{-5}$	$1.09 \cdot 10^{-4}$	$2.87 \cdot 10^{-5}$	$2.33 \cdot 10^{-4}$	$4.20 \cdot 10^{-5}$

6. Activation energy calculation

From the statistical analysis of the growth isotherms we can conclude that the growth of the P faces is limited by diffusion of the growth units in the solution. Conversely we cannot decide if the growth of the N faces is limited by surface diffusion or by both surface and volume diffusion, depending on the solution supersaturation. Therefore we are led to analyze the temperature dependence of the parameters derived from these models.

The activation energy for volume diffusion can be obtained from the values of the volume diffusion coefficients which, at the three crystallization temperatures, are respectively:

$$D_v = D^0\left(1 + \frac{d\log(\gamma_\pm)}{d\log(c)}\right) = (8.15; \ 9.14; \ 10.2) \times 10^{-6} \ \frac{cm^2}{sec}$$

From these values we calculate $-R\frac{\partial \log D_v}{\partial \frac{1}{T}} = 17.14 \ \frac{kJoule}{mole}$ by linear regression.

Subtracting from the latter quantity RT calculated at 292.5 K, we get the activation enthalpy for volume diffusion: $\Delta H^\ddagger_{vdiff} = 14.71 \frac{kJoule}{mole}$.
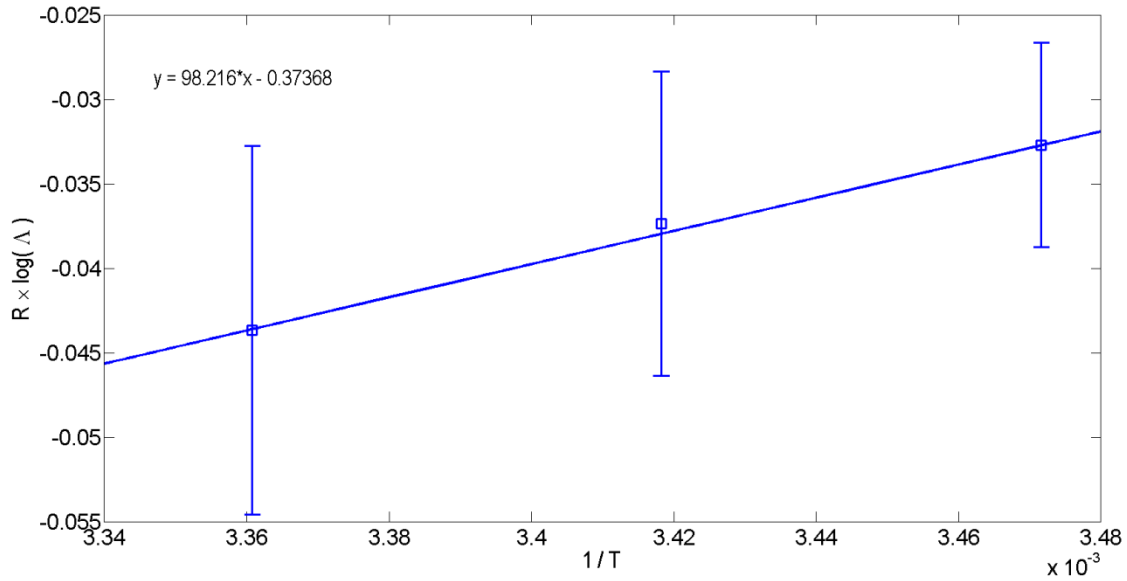
Figure 6. Arrhenius plot of $R\,log\Lambda\,vs\,T^{-1}$ for the faces normal to the solution flow; (see text for details).

From the temperature dependence of Λ we can estimate the value of $\Delta H^{\ddagger}_{desolv}$.

Indeed $\Lambda = a' exp\dfrac{\Delta G^{\ddagger}_{desolv} - \Delta G^{\ddagger}_{vdiff}}{RT}$ can be obtained by fitting the GGC-VS relation to the measured growth rates shown in Figure 6. Λ is considered unaffected by hydrodynamics.

It is $R\dfrac{\partial \ln \Lambda}{\partial T^{-1}} + \Delta H^{\ddagger}_{vdiff} = \Delta H^{\ddagger}_{desolv} = 113.9\dfrac{kJ}{mole}$. This figure seems acceptable if compared with the standard hydration enthalpy of the couple Na^{+}, NO_3^{-} of $728\dfrac{kJ}{mole}$ [31]

As $\Delta H_{des} = \Delta H^{\ddagger}_{des} - \Delta H^{\ddagger}_{desolv}$, a lower bound is obtained: $\Delta H^{\ddagger}_{des} = \Delta H^{\ddagger}_{desolv}$.

6.1 Faces normal to the solution flow: the isotherms (R^{N}_{104} vs σ).

Concerning the growth of the N faces, we consider, at first, the dependence of the parameter p_1 on temperature (Fig. 7) obtaining by the Arrhenius plot the related activation and equilibrium energies. The value of p_1 is related to the slope of R^{N}_{104} at high σ values; p_1 is constrained better than p_2 , which is related to the growth rate at very low supersaturation where accurate measurements are difficult. The temperature dependence is expressed by the equation:

$$-R\dfrac{\partial \ln p_1}{\partial \frac{1}{T}} = RT + \Delta H^{\ddagger}_{des} + \Gamma^{0}_{1}s^{0}_{2}\Delta H^{0}_{1des} + \Delta H^{\dagger}_{ks} \qquad (7)$$
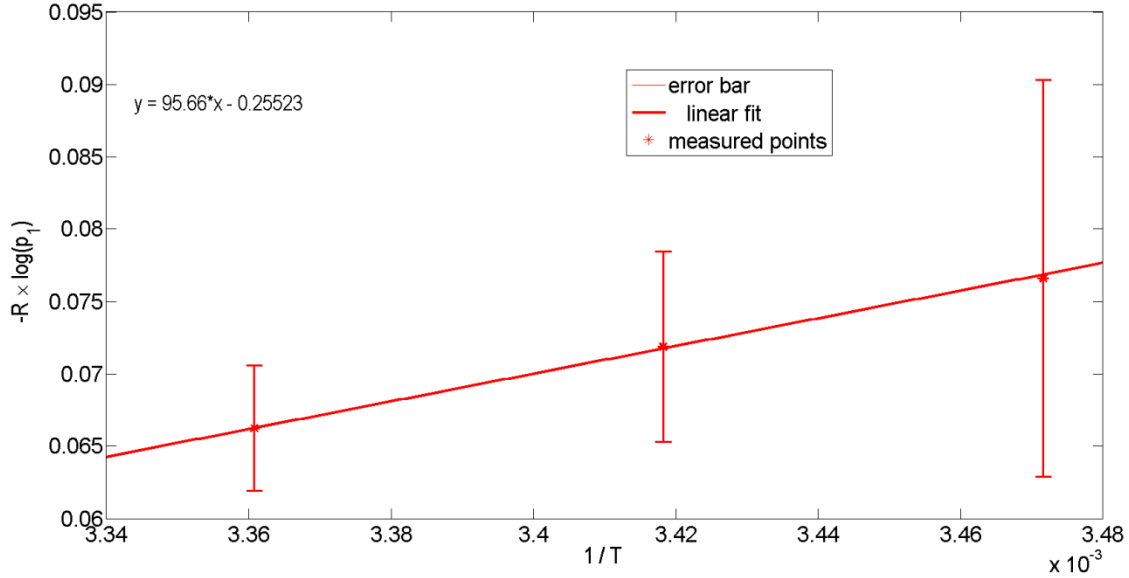
Figure 7. Arrhenius plot of ($R \ log \ p_1$ vs T^{-1}) for the faces normal to the solution flow (see text for details).

This comes from the definition of the parameter $p_1 = \frac{n_{so}}{\tau}\Omega$ (where the molecular volume Ω is a constant) as we calculate:

(a) the variation of the residence time (τ) with T : $-R\frac{\partial ln\tau^{-1}}{\partial\frac{1}{T}} = RT + \Delta H^{\ddagger}_{des}$, where $\Delta H^{\ddagger}_{des}$ represents the activation heat for desorption of a growth unit;

(b) the variation of the concentration of the adsorbed growth units at equilibrium (n_{s0}) with T:

$$-R\frac{\partial ln(n_{so})}{\partial\frac{1}{T}} = \Gamma^0_1 s^0_2 \Delta H^0_{1des} + \Delta H^{\dagger}_{ks}$$

where $\Delta H^{\dagger}_{ks}$ is the mean enthalpy to transfer one growth unit (component 2) from the kink [2] to the surface: on the surface the growth units occupy the area s^0_2 and they can be adsorbed if, simultaneously, $\Gamma^0_1 s^0_2$ molecules of solvent are desorbed with evolution of $\Gamma^0_1 s^0_2 \Delta H^0_{1des}$ joules. Several equations have been proposed for the dependence of n_{s0} on temperature (see ref. [30,32]). We chose that from the Lundager Madsen's thermodynamical model of the adsorbed layer. [32]

It is a quite difficult task to calculate *a priori* $\Gamma^0_1 s^0_2 \Delta H^0_{1des} + \Delta H^{\dagger}_{ks}$, for an adsorbed layer of electrolyte, [32, 33] but we know that it is positive, at least. To estimate this enthalpies we can use the experimental value: $-R\frac{\partial ln \ p_1}{\partial\frac{1}{T}} = 95.66 \frac{kJ}{mole}$, as shown in fig. 6. As we assumed $\Delta H^{\ddagger}_{des} = 113.9 \frac{kJ}{mole}$ we obtain $\Gamma^0_1 s^0_2 \Delta H^0_{1des} + \Delta H^{\dagger}_{ks} < 0$.

We consider now the parameters common to both BCF-S and GGC-VS equations and use $\bar{p}$, the mean value of p_2 and t_2 : at 297.5 K, $\bar{p} = 0.0058 = \frac{\varepsilon \ \gamma a^2}{c \ kTx_s}$, to estimate γ, the mean edge free energy of a straight step developing along the $<\bar{4}41>$ direction on (10. 4).

---

[2] The kink, in the case of a (10.4) face of NaNO$_3$ crystal, is composed by 4 growth units (each of composition NaNO$_3$). Hence, it is a complex kink (not monoatomic or monomolecular Kossel kink), i.e. a "non-Kossel kink" recently introduced by Chernov [36] when dealing with the relaxation time needed to the growth units to find their crystallographic (equilibrium) site within the kink structure.

In the expression of $\bar{p}$, ε depends on the number of interacting spirals of the same sign and c is the shape factor approximately equal to 4, for a lozenge shaped island . Here, it is worth remembering that the lozenge shaped island, limited by four equivalent $\langle\bar{4}41\rangle$ sides, is nothing else than the shape of the 2D nucleus: its size determines the spiral step spacing on the growing (10.4) face; consequently, the value of the mean edge free energy γ concerns both 2D nucleation and spiral growth mechanisms. In general, p_2 depends on the shape of the growth spirals and on their configuration, i.e. if the spirals are isolated or interlaced.[34,35] The simple expression of p_2 we use is suitable to obtain an estimate of γ. Assuming the mean free path of the growth units on (10.4) equal to $4 \cdot 10^{-6}$ cm we calculate $\gamma = 0.47 \times 10^{-6}$ erg cm^{-1}. This value has the correct order of magnitude.

Summing up and according to the bottom of section 5.1.2, hydrodynamic factors and surface features at the nano-scale can explain both the dispersion of the growth rates and that the growth of faces of different orientation may be limited by different elementary processes i.e. their growth can occur with different mechanisms. Notwithstanding the dispersion, the processes limiting the growth rate can be identified, as the experimental (R_{hkl} vs σ) isotherms can be fitted by curves corresponding to proposed growth models and the derived activation energies for growth are supporting the statistical analysis. In conclusion, we accept that the growth rate of the {10.4} faces perpendicular to the solution flow is likely limited by surface diffusion at low supersaturation and, with increasing supersaturation, is limited by volume diffusion, as described by the GGC-VS equation.

6.2 Faces parallel to the solution flow: (R^P_{104}).

Similarly to what we did with the perpendicular faces, here we describe the thermodynamic parameters that can be extracted from the linear law. In figure 8, an Arrhenius plot for the a coefficients is drawn. The experimental activation energy $(E_l^{\ddagger})$ turns out to be 52. 23 kJ/mole.
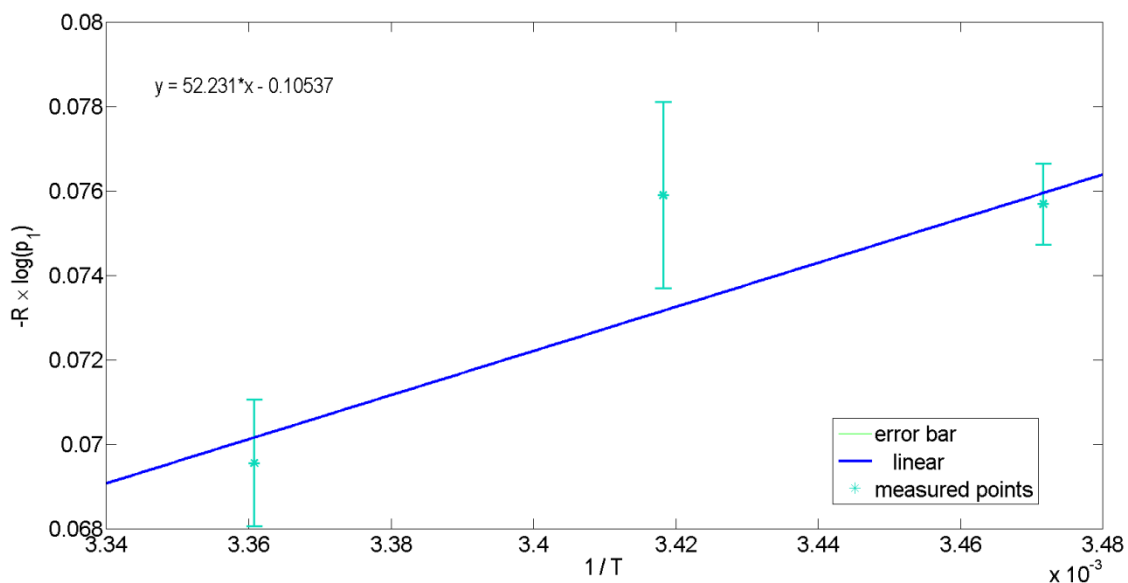
Figure 8. Arrhenius plot for determining the activation energy for $NaNO_3$ crystallization on the faces parallel to the solution flow.

Being $a = \frac{N_0\,\Omega D}{\delta + \Lambda}$, the expression of the activation energy associated to the growth in the linear region is:

$$E_l^{\ddagger} = -R\left\{\frac{\partial \log N_0}{\partial \frac{1}{T}} + \frac{\partial \log D_v}{\partial \frac{1}{T}} - \frac{1}{\delta + \Lambda}\left[\frac{\partial \delta}{\partial \frac{1}{T}} + a'\frac{\Delta H_{desolv}^{\ddagger} - \Delta H_{vdiff}^{\ddagger}}{R} exp \frac{\Delta G_{desolv}^{\ddagger} - \Delta G_{vdiff}^{\ddagger}}{RT}\right]\right\} \quad (8)$$

where $\Delta H_{desolv}^{\ddagger}$ and $\Delta G_{desolv}^{\ddagger}$ are the activation enthalpy and free enthalpy a growth unit surmounts in the transition from the solution to the crystal face.

The first factor can be further developed:

$$-R\frac{\partial \log N_0}{\partial \frac{1}{T}} = -R\left\{\frac{\partial \log m}{\partial \frac{1}{T}} + \frac{\partial \log \rho}{\partial \frac{1}{T}} - \frac{M \times 10^{-3}}{1 + mM \times 10^{-3}}\frac{\partial m}{\partial \frac{1}{T}}\right\}$$

where M is the molecular weight of the solute. The derivative of m are calculated using the solubility by Archer [17]:

$$R\frac{M \times 10^{-3}}{1 + mM \times 10^{-3}}\frac{\partial m}{\partial T^{-1}} = -0.0638 \quad \text{and} \quad -R\frac{\partial \log m}{\partial T^{-1}} = 6.343.$$

The temperature dependence of ρ is calculated from the data by NIST: [17]

$$-R\frac{\partial \log \rho}{\partial T^{-1}} = -0.455 \times 10^{-3}$$

The mean value of $(\delta + \Lambda) = 0.0240$ cm is calculated from the isotherm at 292.5 K. The boundary layer dependence with temperature turns to be: $\frac{\partial \delta}{\partial \frac{1}{T}} = -4.1071$ cm×K, evaluated through the experimental values of solution flow rate (v), mean dimension of crystals (d) and data from NIST[17] to calculate the remaining quantities in the just quoted relation: $\delta = \frac{3}{2}(\frac{kT\rho}{6\pi r\eta^2})^{\frac{1}{3}}(\frac{\eta d}{\rho v})^{\frac{1}{2}}$.

We cannot estimate $\Delta G_{desolv}^{\ddagger} - \Delta G_{vdiff}^{\ddagger}$, as an entropy difference is involved: if the jump distance, a', of a growth unit in solution is $a' \approx 1.10^{-8}$cm, using the experimental value of $E_l^{\ddagger}$ and substituting the calculated quantities in eq.(8), it results $\Delta S_{desolv}^{\ddagger} - \Delta S_{vdiff}^{\ddagger} = 291.8 \frac{J}{mole\,K}$ at 292.5K.

The difference between the activation entropy for partial desolvation of the growth units entering the adsorbed layer and that for volume diffusion is an indication that desolvation brings about an higher disorder than diffusion where ions conserve the hydration shell.

Therefore, considering that during growth: i) the P faces remain flat at the observation under the optical microscope and do not experience effects due to turbulent flow; ii) the shape of the growth isotherms is linear; iii) the thermodynamic analysis do not lead to inconsistencies; then we accept that the growth rate of the P faces is limited by the diffusion in the bulk of the solution.

Conclusions

We have determined the normal growth rate of {10.4} faces of nitratine ($NaNO_3$) single crystal under two different hydrodynamic settings and isothermal conditions in the temperature interval 288 – 297.5 K. In this system, the temperature control is essential because the growth rate of nitratine is very sensitive to the experimental parameters, owing to its elevated solubility. Accordingly, we have constructed a device to overcome all the difficulties. The statistical analysis of the growth isotherms coupled with a thermodynamic study allowed us to assess the rate determining steps of the growth rates of the {10.4} faces of nitratine: volume (P faces) or surface diffusion and volume diffusion (N faces) can limit their growth depending on the prevailing hydrodynamic conditions; conversely, the integration of the growth units in the steps is not rate limiting. Likewise, we estimated the edge energy of steps on {104}. Some activation quantities related to the transfer of growth units from kinks and from solution to the adsorbed layer could also be estimated. Both the experimental set up and the measurement method allowed us to overcome the drawbacks which are intrinsic not only to nitratine, but usually to all very soluble compounds. The promising results we are obtaining from the observation of the growing surfaces by *in - situ* confocal and atomic force microscopy, make us confident of acquiring deeper insight about the crystallization of nitratine.

REFERENCES

(1) Paul, G. L.; Pryor, A. W. *Acta Cryst.* **1972**, *B 28*, 2700-2702.

(2) Benages-Vilau, R.; Costa, E.; Bruno, M.; Cuevas-Diarte, M. A.; Calvet , T.; Aquilano, D. *Cryst. Res. Technol*.**, 2011**, *46(8)*, 773 – 778.

(3) Sipyagin, V.; Chernov, A. *Kristallografiya* **1972**, *17 (5)*, 1003-1012.

(4) Kirkova, E.; Nikolaeva, R. *Cryst. Res. Technol.* **1983**, *18 (6)*, 743-754.

(5) Treivus, E. B. *Cryst. Res. Technol.* **1997**, *32 (7)*, 963-972.

(6) Jones, C. M.; Larson, M. A. *AIChE J.* **1999**, *45 (10)*, 2128-2135.

(7) Jones, C. M.; Larson, M. A. *Chem.Eng. Science***, 2000**, *55 (14)*, 2563-2570.

(8) Jones, C. M.; Larson, M.A.; Ristic, R.I.; Sherwood, J.N. *J. Cryst. Growth*, **2000**, *208(1-4)*, 520-525(9) Ristic, R. I.; Shekunov B. Yu.; Sherwood, J. N. *J. Cryst. Growth***, 1997**, *179*, 205-212.

(10) Ristic, R. I.; Sherwood, J. N.; Shripathi, T. *J.Cryst.Growth***, 1997**, *179*, 194-204.

(11) Graber, T. A.; Taboada, M. E.; Alvarez, M. N.; Schmidt, E. H. *Cryst. Res. Technol.*, **1999**, *34 (10)*, 1269-1277.

(12) Oosterhof, H.; Geertman, R.M.; Witkamp, G.J.; van Rosmalen, G.M. *J. Cryst. Growth*, **1999**, *198-199(part1)*, 754-759. (13) Komnik, S. N.; Startsev, V. I. *J. Cryst. Growth*, **1969**, *5*, 207-209.

(14) Gopalakhrishnan, R.; Arivuoli, D.; Ramasamy, P. *Cryst. Res. Technol.* **1991**, *26 (6)*, K141-K146.

(15) Sawada, T.; Schichiri, T. *J. Cryst. Growth*, **1984**, *67(2)* , 233-240

(16) Rubbo, M.; Sherwood, J.N. *J.Cryst.Growth*, **1983**, *61*, 210-214.

(17) Xu, T.; Pruess, K. *Thermophysical Properties of Sodium Nitrate and Sodium Chloride Solutions and their Effects on Fluid Flow in Unsaturated Media.* **2001**. E. O. Lawrence Berkeley National Laboratory, Berkeley, CA (US). DOI 10.2172/790019 .

(18) Archer, D. G. *J. Phys. Chem. Ref. Data*, **2000**, *29(5)*, 1141.

(19) Beckmann, W.; Boistelle, R.; Sato, K. J. Chem. Eng. Data, **1984**, *29*, 211-214.

(20) Gilmer, G.; Ghez, R.; Cabrera, N. *J.Cryst.Growth* **1971**, *8(1)*, 79-93.

(21) Burton, W. K.; Cabrera, N. Frank, F. C. *Phil. Trans. Roy. Soc. A*, **1951**, *243 (866)*, 299-358.

(22) Bennema, P.; Gilmer, G. in *Crystal growth: an introduction*. Hartman, P. ed., Amsterdam: North-Holland, 1973, 263-327.

(23) Chernov, A. A. Soviet Phys. Uspekhi, **1961**, *4(1)*, 116-148.

(24) Robinson, R. A. ; Stokes, R. H. *Electrolyte Solutions.* , 2nd Rev. Ed. Dover Books on Chemistry, 2002, Ch. 11 and App. 6.2.

(25) Brandt , S. *Statistical and Computational Methods in Data Analysis*, North Holland, Amsterdam, 1970(26) Carlson, A. in: *Growth and Perfection of Crystals*, Eds. R. H.. Doremus, B. W. Roberts and D. Turnbull (Wiley, New. York, 1958) p. 421-426

(27) Bedarida, F.; Zefiro L.; Boccacci, P.; Aquilano, D.;Rubbo,M.; Vaccari, G.; Mantovani, G.; Sgualdino, G. *J. Cryst. Growth*, **1988**, *89(4)*, 395-404

(28) Benages-Vilau, R. (unpublished results)

(29) Rubbo, M. *J. Cryst. Growth*, **2006**, 291(2), 512-520

(30) a) Frank, F.C. in *Growth and Perfection of Crystals* p.411; b) Cabrera, N.; Vermilyea, D.A. in *Growth and Perfection of Crystals* p.393. Eds. R. H.. Doremus, B. W. Roberts, D. Turnbull (Wiley, New. York, 1958)

(31) Marcus, Y. *J. Chem. Soc. , Faraday Trans.* , **1987**, 83, 339-349

(32) Lundager Madsen, H. E. *J. Cryst. Growth*, **1977**, *39*, 250-254.

(33) Lundager Madsen, H. E. *Cinétique de Croissance des Faces (001) des cristaux d' Hexatriacontane en Solution.* , 1978, Thèse, Université Aix-Marseille III .

(34) Rubbo, M.; Aquilano, D. *Atti Accad. Sci. Torino***, 1976**, 119-136*.*

(35) Chapon, C.; Bonissent. A. *J.Cryst.Growth***, 1973**, 18 (1), 103-106.

(36) a) Chernov, A.A. ; Rashcovich, L.N.; Vekilov, P.G. *J.Cryst.Growth***, 2005,** 275(1-2) pp. 1-18; b) Chernov A. A., Petrova E. V., and Rashkovich L. N. (2006) *J. Cryst. Growth,* **2006,** 289, 245–254.